Letter | Editors' Suggestion

Optical switch of electron-hole and electron-electron collisions in semiconductors

Yang Wang,[1] Yu Liu,[1] Pengzuo Jiang,[1] Yunan Gao,[1,2,3,4] Hong Yang,[1,2,3,4] Liang-You Peng,[1,2,3,4] Qihuang Gong,[1,2,3,4] and Chengyin Wu[1,2,3,4,*]

[1]*State Key Laboratory for Mesoscopic Physics and Frontiers Science Center for Nano-optoelectronics, School of Physics, Peking University, Beijing 100871, China*

[2]*Collaborative Innovation Center of Quantum Matter, Beijing 100871, China*

[3]*Collaborative Innovation Center of Extreme Optics, Shanxi University, Taiyuan, Shanxi 030006, China*

[4]*Peking University Yangtze Delta Institute of Optoelectronics, Nantong, Jiangsu 226010, China*

(Received 17 January 2023; revised 30 March 2023; accepted 31 March 2023; published 11 April 2023)

We investigate the ultrafast carrier dynamics in a ZnO crystal irradiated by a strong, linearly polarized midinfrared laser pulse. Depending on the laser intensity, there exist two dominant light wave-driven processes, i.e., the electron-hole collision recombination and the electron-electron impact excitation. The corresponding optical signatures are high-order harmonic generation and stimulated emission, respectively. By adding a weak infrared or telecom wavelength laser pulse with an orthogonal polarization, we show that these two carrier dynamic processes can be effectively controlled by tuning the time delay between the two laser pulses. This all-optical control has an ultrafast speed, a low threshold, and a broad spectral responsiveness, which have implications in understanding the ultrafast carrier dynamics in the condensed matter and the design of next-generation optoelectronic switches.

DOI: 10.1103/PhysRevB.107.L161301

Optoelectronic information devices are being developed to achieve ultrafast speed, an ultrasmall size, and ultralow power consumption. The rate of signal processing and sampling is determined by the switching time of the transient current [1]. Light wave–driven electronic devices with ultrashort lasers can overcome the limits of conventional transistor-based electronics and push the electronic signal processing and sampling rate into the petahertz (10^{15} Hz) frequency regime [2–4]. The interaction of a strong ultrashort laser with gaseous atoms and molecules has been extensively investigated. It has opened the door to observing and controlling the motion of electrons with a subatomic resolution in both space and time domains [5,6]. In the past decade, the interaction of a strong ultrashort laser with matter has been extended to the condensed phase [7–11]. Such an interaction can control the electron dynamics on the subcycle timescale and provides a promising candidate for photo-controlled switching and electron sampling. However, the applied laser intensity of higher than $10\,\mathrm{TW/cm^2}$ limits its practical application due to the low damage threshold of the condensed matter. The interaction of a strong ultrashort laser with the condensed matter is far more complicated. The excited carriers have multiple interactions, such as the electron-hole (e-h) recombination [10,12], electron-electron (e-e) collision [13–15], and electron-phonon scattering [16,17]. Understanding the laser-induced, ultrafast nonequilibrium carrier dynamics and controlling them with weak laser pulses is pivotal for designing and developing next-generation optoelectronic devices [18].

Solid-state high-order harmonic generation (HHG) involves electron motion in strong laser fields and provides an ultrafast probe to monitor the carrier dynamics within the subcycle temporal resolution [18–21]. In 2011, Ghimire *et al.* [7] reported the experimental observation of nonperturbative HHG in ZnO bulk crystals and opened the door to studying HHG in solids. Irradiated by a midinfrared (MIR) femtosecond laser with photon energy much smaller than the bandgap, electrons in the valence band are excited to the conduction band, leaving associated holes in the valence band. Driven by the oscillating laser electric field, electrons and holes are accelerated along the corresponding bands. High-order harmonic (HH) photons are emitted due to the nonlinear currents in the individual bands or the collision recombination of the electron with its associated hole. The relative contribution of the so-called intraband and interband HH depends on the laser parameters as well as the band structures of the solid sample [22]. Very recently, the e-e impact excitation process was identified in polycrystalline ZnO thin film by strong MIR laser fields [15]. Once the energy of the electron in the conduction band obtained from the laser field is larger than the bandgap energy, the e-e impact excitation promotes a bound electron from the valence band to the conduction band and results in stimulated emission (SE) in the near-ultraviolet spectral range. Electron multiplication caused by the e-e impact excitation has been reported for the zero-bandgap monolayer graphene, which takes place in the early stage of electron thermalization. These properties make graphene an ideal material in photovoltage generation and photon detection [14]. However, the requirement is too critical for the electron multiplication in semiconductors. The e-e impact excitation requires that the electron energy be larger than

*Corresponding author: cywu@pku.edu.cn

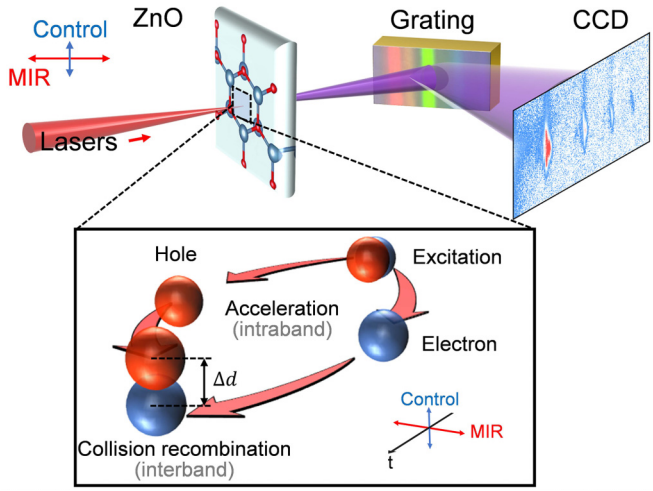

FIG. 1. Emission spectrum measurement of ZnO irradiated by a two-color laser with orthogonal polarization. The inset illustrates the underlying mechanism for a weak control laser that introduces a transverse displacement to suppress the e-h collision recombination.

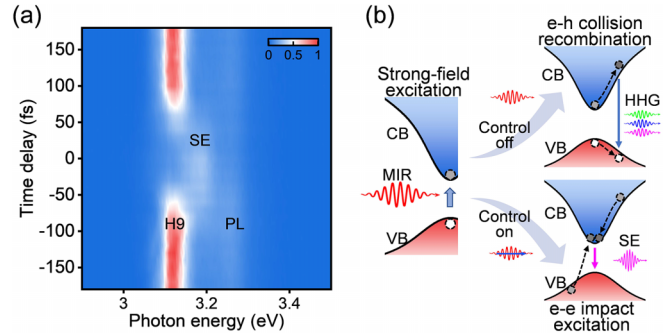

FIG. 2. Interaction of ZnO with a two-color laser. (a) Emission spectra as a function of the time delay between the two laser pulses with orthogonal polarization. (b) The control scheme for the ultrafast switch from the e-h collision recombination to the e-e impact excitation.

the bandgap energy, in accordance with energy conservation [15,23].

In this Letter, we experimentally investigate the ultrafast carrier dynamics of a ZnO crystal irradiated by a strong MIR laser. Two light wave–driven carrier dynamic processes are monitored through measuring corresponding optical signatures. One is the e-h collision recombination, which leads to HHG around and above the bandgap. The other is the e-e impact excitation, which leads to SE near the bandgap. By using another orthogonally polarized weak laser in the telecom or the infrared wavelength range, we demonstrate the precise control of these two carrier dynamic processes on a timescale of a few hundred femtoseconds with a threshold intensity of $3.4\,\mathrm{GW/cm^2}$. This all-optical switch in the condensed matter has an ultrafast speed, a low threshold, and a broad spectral responsiveness. It can be potentially integrated into chips and boost the speed of optoelectronic information devices into the tens of terahertz region.

In Fig. 1, we show the schematic diagram of the experimental setup. The 800-nm femtosecond laser pulse launched from a Ti:sapphire amplifier is introduced into an optical parametric amplifier (OPA) to generate a wavelength-tunable near-infrared (NIR) laser (1.1 to 2.6 μm). A MIR laser (3 to 9 μm) is further generated through the collinear difference frequency between the signal and idler beams of the OPA. The MIR laser and the NIR laser are collinearly combined with a dichroic mirror, and the time delay is controlled by a Michelson interferometer configuration. Measurements are performed on a 350-μm-thick (0001) ZnO crystal with an energy difference between the valence and conduction bands that is quasi-isotropic in the center of the Brillouin zone. The strong MIR laser creates e-h pairs through strong field excitation. During the laser-driven e-h pair acceleration, an additional perturbation in the vertical direction caused by the weak control laser generates a transverse displacement and suppresses the e-h collision recombination. It should be noted that the control laser is too weak to excite the electron alone.

We measured the emission spectra of ZnO irradiated by the 3.5-μm MIR laser with various intensities. The laser pulse duration is about 80 fs. In addition to typical HH peaks, the photoluminescence (PL) due to the spontaneous emission and SE can be identified at around 3.2 eV. The relatively intensity between HH and SE strongly depends on the laser intensity of the MIR laser. When the laser intensity is below $0.9\,\mathrm{TW/cm^2}$, HH dominates. While the laser intensity is above $1.5\,\mathrm{TW/cm^2}$, SE becomes dominant. It should be mentioned that HH is linearly polarized as the pump laser. While the polarization of SE is anisotropic, the ratio is about two between the parallel component and the vertical component. The polarization is isotropic for PL. In Fig. 2, the MIR pump laser is fixed around $1.3\,\mathrm{TW/cm^2}$. When the pump laser is applied alone, the ninth HH (H9) and PL are exhibited around the bandgap. When the weak 1.3-μm telecom wavelength control laser is further injected, the spectra strongly depend on the time delay between the two lasers. When the two lasers do not overlap in time, the spectrum is the same as that of the MIR laser alone. In contrast, when the two lasers overlap in time, the SE peak appears and becomes stronger. In the meantime, HH peaks quickly diminish.

According to the semiclassical framework [22], the solid HHG originates from an intraband current or an interband current. The intraband current is caused by the strong laser field-driven dynamic oscillation of electrons and holes within individual bands. The interband current is the result of the collision recombination of the electron with its associated hole. It has been shown that interband harmonics are sensitive to the trajectories and strongly depend on the e-h coherence [24–26]. The transverse displacement induced by the control laser can suppress the e-h collision recombination [27]. In contrast, such displacement has a negligible effect on intraband harmonics, especially in the isotropic region of the energy band [28]. Hence, the responses to the orthogonally polarized control laser can serve as sensitive probes for distinguishing the intraband and interband contributions. The observed large attenuation of the harmonic intensity shows that interband harmonics play the dominant role. This conclusion is consistent with our simulation that the interband contribution is about two orders of magnitude higher than that of the intraband contribution [29]. The interband HHG results

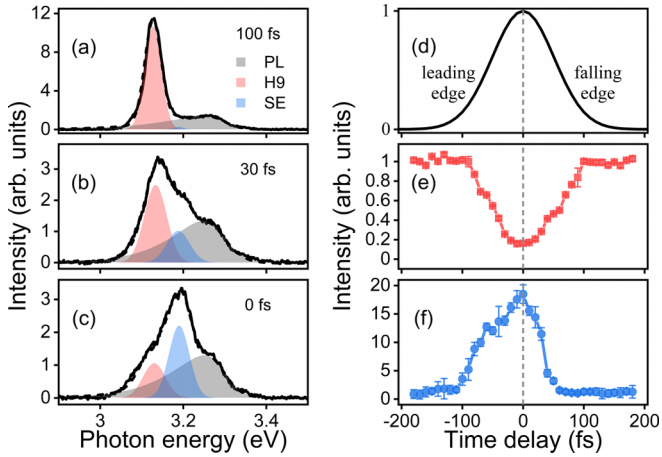

FIG. 3. Spectral shape and integrated intensity as a function of the time delay between the two-color laser pulses. Emission spectrum around the bandgap at three different delays: (a) 100 fs, (b) 30 fs, and (c) 0 fs. (d) Envelope of the strong mid-infrared pump laser. Spectral integrated intensity of (e) H9 and (f) SE versus the time delay of the two-color laser pulses.

from a subcycle ultrafast electron-hole collision. The efficiency of the collision recombination can be modulated by the weak orthogonally polarized laser field, which is reflected by the detectable optical signatures. The e-h collision recombination is efficiently suppressed by the transverse misalignment generated by the orthogonally polarized laser field. The maximum of the transverse misalignment Δd is proportional to $E\lambda^2/4\pi^2mc^2$ [7], where E and λ are the peak amplitude and the wavelength of the control laser, respectively. Under our experimental conditions, Δd is estimated to be less than 0.2 Å. Such a transverse misalignment between the electron and the hole is small compared to the spatial drift (∼20 Å) induced by the MIR laser and the lattice constant (4.4 Å) of ZnO. Figure 2(b) illustrates the control scheme. When the MIR laser is applied, e-h pairs are created and accelerated by the strong laser field. The e-h collision recombination leads to HHG. When a control laser with an orthogonal polarization is further applied, it can induce a transverse misalignment and greatly suppress the e-h collision recombination. As a result, the harmonic intensity is decreased. At the same time, the surviving electrons continue to be driven and accelerated by the strong MIR laser field. Once the energy of the electron in the conduction band is larger than the bandgap energy, the e-e impact excitation can promote a bound electron from the valence band to the conduction band. These electrons in the conduction band will be accelerated by the strong MIR laser in the next optical cycle, which leads to the electron multiplication. When the population inversion is built, the near-ultraviolet SE is subsequently generated.

We have demonstrated that the weak control laser with an orthogonal polarization can switch the e-h collision recombination to the e-e impact excitation. This switch is ultrafast and depends on the time delay between the two laser pulses. In Fig. 3(a)–3(c), we present the integrated spectra at three typical delays. The spectra are fitted with three functions to distinguish the contribution of H9 (red), SE (blue), and PL (gray). When the control laser is behind the MIR laser (delay = 100 fs), H9 and PL are both clearly observed. The spectrum is essentially the same as that of the MIR laser alone. When the two lasers partially overlap in time (delay = 30 fs), the SE peak appears between H9 and PL, accompanied by the significant attenuation of H9. When the two lasers overlap completely (delay = 0 fs), the H9 intensity is decreased by one order of magnitude. Concurrently, the SE peak reaches its maximum and becomes the major component. This shift from HH to SE signifies the switch from the e-h collision recombination to the e-e impact excitation. The weak control laser has served as an optical switch. In Fig. 3(d)–3(f), we show the evolution of the integrated intensity of H9 and SE as a function of the time delay between the two laser pulses. As depicted in Fig. 3(e), the H9 attenuation reaches maximum at zero delay. The harmonic intensity is symmetrically distributed for a positive and a negative delay, exhibiting a Gaussian shape attenuation. This measurement implies that both the strong MIR and the weak control laser maintain a Gaussian envelope without introducing any pulse-shaping effects during the propagation. As shown in Fig. 3(f), the SE intensity increases with the overlap of the two laser pulses and reaches the maximum enhancement factor of almost 20 when the two lasers entirely overlap. In contrast to the harmonic attenuation, the SE enhancement on both sides of the pulse center exhibits an asymmetric distribution, with a leading edge of about 100 fs and a falling edge of almost 50 fs. It should be emphasized that the data in Fig. 3(e) and 3(f) are taken from the same record, which eliminates the influence of the measurement on the symmetry differences between H9 and SE.

The different distributions of SE and H9 intensity with respect to the leading and falling edges of the MIR pump laser can be explained by the corresponding carrier dynamics. Harmonics are generated through the e-h collision recombination and repeat every half cycle of the MIR pump laser. The introduction of the orthogonally polarized control laser suppresses the e-h collision recombination, resulting in a symmetric distribution of the harmonic attenuation with respect to the positive and negative delays. However, SE is generated through the e-e impact excitation, which requires electrons to obtain enough energy from the MIR laser field to overcome the bandgap. The average energy of free electrons in an oscillating electric field is proportional to the laser intensity. When the control laser is injected at the leading edge of the MIR pump laser, the electron that has survived from the e-h collision recombination can be further accelerated. Once the electron energy obtained from the MIR laser field is greater than the bandgap, the e-e impact excitation can be greatly enhanced. The excited electrons in the conduction band are further accelerated by the MIR laser field. The process repeats and leads to the electron multiplication. Once the population inversion is built, the SE will be greatly enhanced. However, when the control laser is injected at the falling edge of the MIR laser, the electron that has survived from the e-h collision recombination cannot be efficiently accelerated due to the decrease of the laser intensity at the falling edge. If the electron energy obtained from the MIR laser field does not exceed the bandgap energy, the e-e impact excitation cannot occur. As a result, the enhanced SE intensity is no longer symmetrically distributed relative to the peak value of the MIR pump laser.

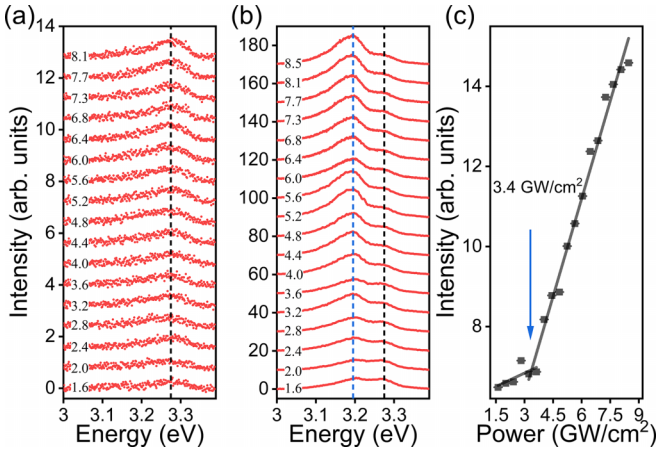

FIG. 4. Emission spectra around the bandgap at different intensities for both the pump laser and the control laser. A grating polarizer has been utilized to filter the harmonics out. The control laser intensity is marked by the numerical number at each curve in units of gigawatts per square centimeter. (a) The pump laser intensity is $0.9\,\mathrm{TW/cm^2}$. (b) The pump laser intensity is $1.3\,\mathrm{TW/cm^2}$. (c) Spectra intensity of (b) as a function of the power of the control laser, from which a threshold intensity can be clearly determined.

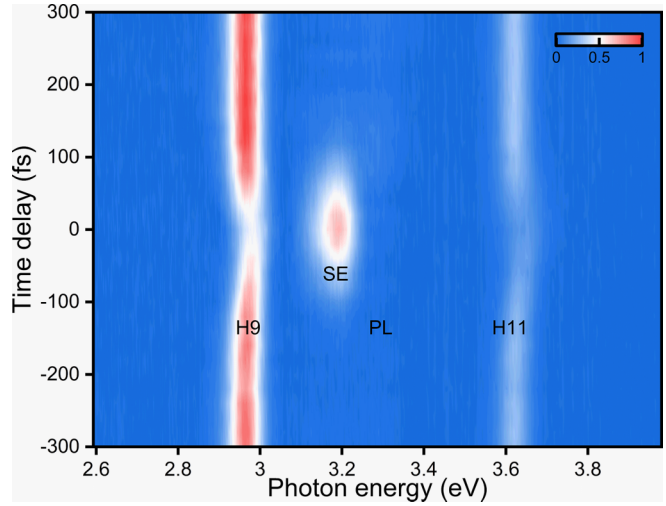

FIG. 5. Emission spectra of ZnO as a function of the time delay between the two laser pulses with orthogonal polarization. The intensity is $1.3\,\mathrm{TW/cm^2}$ and the wavelength is 3.75 μm for the pump laser, while the intensity is $50\,\mathrm{GW/cm^2}$ and the wavelength is 800 nm for the control laser.

In the experiment of two-color laser fields with orthogonal polarization, the electron energy obtained from the MIR pump laser depends on the time delay between the two laser pulses. In the following, we fix the time delay at zero but vary the intensity of the MIR pump laser to control the energy the electron obtained from the MIR pump laser. The results are shown in Fig. 4, where a grating polarizer is utilized to filter the harmonics out by the polarization selection. When the MIR laser intensity is around $0.9\,\mathrm{TW/cm^2}$, the maximum energy the electron obtained from the laser field is just lower than the bandgap of 3.2 eV, which is inadequate to trigger the e-e impact excitation channel. Under this condition, the e-h collision recombination is still suppressed with the introduction of the orthogonally polarized control laser. As a result, the PL intensity of the spontaneous radiation increases monotonically with the increase of the control intensity. In contrast, when the MIR laser intensity is $1.3\,\mathrm{TW/cm^2}$, the maximum energy the electron obtained from the laser field is around 4.7 eV, which is much greater than the bandgap. The injection of the control laser can switch the e-h collision recombination to the e-e impact excitation. As the control laser intensity is increased, the SE peak appears and becomes the dominating component of the spectrum. Figure 4(c) depicts the dependency of the spectral intensity of Fig. 4(b) on the control laser intensity. The difference in the intensity scaling between the low and high laser intensity regions indicates the switch from the e-h collision recombination to the e-e impact excitation channel. The switching threshold is around $3.4\,\mathrm{GW/cm^2}$. Our result indicates that an ultrasensitivity of the all-optical switch can be realized through manipulating the e-h and e-e collision with a weak control laser.

Last but not least, we have also carried out the measurement with various wavelengths for both the pump laser and the control laser. Our results show that the ultrafast switch can operate over a wide range of the control laser wavelength. In Fig. 5, we show the emission spectra as a function of the time delay between the two laser pulses. The pump laser has a wavelength of 3.75 μm and an intensity of $1.3\,\mathrm{TW/cm^2}$; the control laser has a wavelength of 800 nm and an intensity of $50\,\mathrm{GW/cm^2}$. It can be seen that the switch can also operate, but with a slight increase in the threshold intensity of the control laser. The qualitative consistency for the control laser with different wavelengths suggests that the ultrafast switch can operate over a wide variety of wavelengths and has a broad spectral responsiveness.

In conclusion, we have provided an all-optical method to observe and control the ultrafast carrier dynamics in semiconductors. The light wave–driven e-h collision recombination and e-e impact excitation are identified by measuring the spectrum intensity of HH and SE. We demonstrate that these two processes can be efficiently controlled by a weak control laser with an orthogonal polarization. The control of the e-h collision recombination and the e-e impact excitation can serve as an ultrafast all-optical switch. It has an ultrafast switching speed and reaches 10 THz (100 fs) for the leading edge and 20 THz (50 fs) for the falling edge. The threshold intensity is $3.4\,\mathrm{GW/cm^2}$ for the 1.3-μm telecom wavelength laser. In addition, this ultrafast all-optical switch has a broad spectral responsiveness. These properties make the ultrafast switch have potential applications for next-generation optoelectronic information devices. It can potentially be integrated into chips and boost the speed of optoelectronic information devices into the tens of terahertz region.

This work was supported by National Key R&D Program of China (Grants No. 2018YFA0306302 and No. 2022YFA1604301) and the National Natural Science Foundation of China (Grants No. 12174011, No. 92250305, No. 11527901, No. 12234002, and No. 92250303).

[1] H. J. Caulfield and S. Dolev, Nat. Photonics **4**, 261 (2010).

[2] A. Schiffrin, T. Paasch-Colberg, N. Karpowicz, V. Apalkov, D. Gerster, S. Mühlbrandt, M. Korbman, J. Reichert, M. Schultze, S. Holzner, J. V. Barth, R. Kienberger, R. Ernstorfer, V. S. Yakovlev, M. I. Stockman, and F. Krausz, Nature (London) **493**, 70 (2013).

[3] M. Schultze, E. M. Bothschafter, A. Sommer, S. Holzner, W. Schweinberger, M. Fiess, M. Hofstetter, R. Kienberger, V. Apalkov, V. S. Yakovlev, M. I. Stockman, and F. Krausz, Nature (London) **493**, 75 (2013).

[4] M. Garg, M. Zhan, T. T. Luu, H. Lakhotia, T. Klostermann, A. Guggenmos, and E. Goulielmakis, Nature (London) **538**, 359 (2016).

[5] P. B. Corkum and F. Krausz, Nat. Phys. **3**, 381 (2007).

[6] F. Krausz and M. Ivanov, Rev. Mod. Phys. **81**, 163 (2009).

[7] S. Ghimire, A. D. DiChiara, E. Sistrunk, P. Agostini, L. F. DiMauro, and D. A. Reis, Nat. Phys. **7**, 138 (2011).

[8] H. Liu, Y. Li, Y. S. You, S. Ghimire, T. F. Heinz, and D. A. Reis, Nat. Phys. **13**, 262 (2017).

[9] T. T. Luu, M. Garg, S. Y. Kruchinin, A. Moulet, M. T. Hassan, and E. Goulielmakis, Nature (London) **521**, 498 (2015).

[10] B. Zaks, R. B. Liu, and M. S. Sherwin, Nature (London) **483**, 580 (2012).

[11] F. Langer, M. Hohenleutner, C. P. Schmid, C. Poellmann, P. Nagler, T. Korn, C. Schüller, M. S. Sherwin, U. Huttner, J. T. Steiner, S. W. Koch, M. Kira, and R. Huber, Nature (London) **533**, 225 (2016).

[12] M. Hohenleutner, F. Langer, O. Schubert, M. Knorr, U. Huttner, S. W. Koch, M. Kira, and R. Huber, Nature (London) **523**, 572 (2015).

[13] M. Schultze, K. Ramasesha, C. D. Pemmaraju, S. A. Sato, D. Whitmore, A. Gandman, J. S. Prell, L. J. Borja, D. Prendergast, K. Yabana, D. M. Neumark, and S. R. Leone, Science **346**, 1348 (2014).

[14] D. Brida, A. Tomadin, C. Manzoni, Y. J. Kim, A. Lombardo, S. Milana, R. R. Nair, K. S. Novoselov, A. C. Ferrari, G. Cerullo, and M. Polini, Nat. Commun. **4**, 1987 (2013).

[15] R. Hollinger, E. Haddad, M. Zapf, V. Shumakova, P. Herrmann, R. Röder, I. Uschmann, U. Reislöhner, A. Pugžlys, A. Baltuška, F. Légaré, M. Zürch, C. Ronning, C. Spielmann, and D. Kartashov, Phys. Rev. B **104**, 035203 (2021).

[16] J. C. W. Song, M. Y. Reizer, and L. S. Levitov, Phys. Rev. Lett. **109**, 106602 (2012).

[17] J. Coulter, G. B. Osterhoudt, C. A. C. Garcia, Y. Wang, V. M. Plisson, B. Shen, N. Ni, K. S. Burch, and P. Narang, Phys. Rev. B **100**, 220301(R) (2019).

[18] G. Vampa, T. J. Hammond, N. Thiré, B. E. Schmidt, F. Légaré, C. R. McDonald, T. Brabec, and P. B. Corkum, Nature (London) **522**, 462 (2015).

[19] G. Vampa, C. R. McDonald, G. Orlando, P. B. Corkum, and T. Brabec, Phys. Rev. B **91**, 064302 (2015).

[20] R. E. F. Silva, I. V. Blinov, A. N. Rubtsov, O. Smirnova, and M. Ivanov, Nat. Photonics **12**, 266 (2018).

[21] O. Schubert, M. Hohenleutner, F. Langer, B. Urbanek, C. Lange, U. Huttner, D. Golde, T. Meier, M. Kira, S. W. Koch, and R. Huber, Nat. Photonics **8**, 119 (2014).

[22] G. Vampa, C. R. McDonald, G. Orlando, D. D. Klug, P. B. Corkum, and T. Brabec, Phys. Rev. Lett. **113**, 073901 (2014).

[23] H. Hirori, K. Shinokita, M. Shirai, S. Tani, Y. Kadoya, and K. Tanaka, Nat. Commun. **2**, 594 (2011).

[24] Z. Wang, H. Park, Y. H. Lai, J. Xu, C. I. Blaga, F. Yang, P. Agostini, and L. F. DiMauro, Nat. Commun. **8**, 1686 (2017).

[25] C. Heide, Y. Kobayashi, A. C. Johnson, F. Liu, T. F. Heinz, D. A. Reis, and S. Ghimire, Optica **9**, 512 (2022).

[26] K. Nagai, K. Uchida, S. Kusaba, T. Endo, Y. Miyata, and K. Tanaka, arXiv:2112.12951 (2021).

[27] S. D. C. Roscam Abbing, F. Campi, A. Zeltsi, P. Smorenburg, and P. M. Kraus, Sci. Rep. **11**, 24253 (2021).

[28] Y. Sanari, T. Otobe, Y. Kanemitsu, and H. Hirori, Nat. Commun. **11**, 3069 (2020).

[29] Y. Wang, T. Shao, X. Li, Y. Liu, P. Jiang, W. Zheng, L. Zhang, X.- B. Bian, Y. Liu, Q. Gong, and C. Wu, Opt. Express **31**, 3379 (2023).